Entropy optimization of an additively manufactured heat exchanger with a dual stage Gifford-McMahon cryogenic refrigerator for hydrogen liquefaction

J Raymond, C Bunge, L Pesek, and J Leachman

Hydrogen Properties for Energy Research (HYPER) Laboratory, School of Mechanical and Materials Engineering, Washington State University, Pullman, WA 99164-2920 USA

Jacob.leachman@wsu.edu

Abstract. Small-scale hydrogen liquefaction has emerged as an approach to fuel small aircraft powered by fuel cells. However, limited research on the design and optimization of small-scale hydrogen liquefiers, specifically the heat exchangers, is available. This paper describes a minimum entropy design for a heat exchanger mounted on a dual stage Gifford-McMahon cryogenic refrigerator. To minimize entropy generation the heat exchanger utilizes a bifurcating flow structure with varying wall thickness. Numerical optimization indicates that the heat exchanger will generate half of the entropy of a single coiled tube, significantly reducing the required heat exchanger length by 91.4% and the thermal mass by 43.8%. The heat exchanger was 3D printed with an aluminum alloy and the interior coated with a ruthenium-based catalyst for ortho-parahydrogen conversion. Hydrogen entering the heat exchanger near 293 K and 653 kPa is cooled to 28.1 K and full ortho-parahydrogen conversion is assumed before entering the storage dewar. The resulting experimental tests indicate a potential to increase heat exchanger efficiency in a more compact form factor, as well as a promising future for additively manufactured components in cryogenics.

1. Introduction

Small-scale hydrogen liquefaction is being pursued for fueling small aircraft utilizing fuel cells. However, even large-scale hydrogen liquefiers are notoriously inefficient, operating at only 20-30% of second law efficiency. Little research has been done on small-scale system optimization, and most of what has been completed is only theoretical [1, 2]. Heat exchangers are one of the most inefficient components in the system and experience thermodynamic losses of almost 13% [3]. Common methods of heat exchanger optimization include modifying geometry, utilizing precooling, and adding fins [4-10]. No entropy-based optimizations have been attempted utilizing a branching flow structure.

In this work an entropy optimized, additively manufactured heat exchanger for hydrogen liquefaction is presented. The design utilizes a branching flow structure and a varying wall thickness. The system is mounted onto a dual stage Gifford-McMahon cryogenic refrigerator and additively manufactured out of $AlSi_{10}Mg$. The system is compared to a single tube design and experimental trials are used to quantify the rate of liquefaction and the final temperature profile of the heat exchanger. The results are compared to the theoretical predictions and suggestions are given for future work. A more thorough compilation of this work is available in the Master's thesis by Raymond [11].

2. Theory

Hydrogen was first liquefied by James Dewar in 1898, and since then heat exchangers have been optimized in a multitude of ways [12]. Heat exchangers are typically optimized by decreasing temperature differentials and pressure drops within the system. The ideal temperature profile is linear. The main forms of optimization are geometry modifications, the addition of fins, the use of precooling, and placement of catalyst in hydrogen systems.

An optimum system is defined for this study as one with minimum entropy generation. Heat exchangers typically consist of systems of tubes, and entropy generation within a tube is a function of pressure and temperature differentials. In an ideal system, the outlet pressure is the same as the inlet and the outlet temperature is the same as the surface temperature. In Figure 1, the inlet state is point 1, the outlet state is point 2, and the ideal outlet state is point 2'. Entropy generation from the pressure gradient is due to the difference between P_{in} and P_{out}, and entropy generation from the temperature gradient is due to the difference between the temperature at point 2 and T_s.

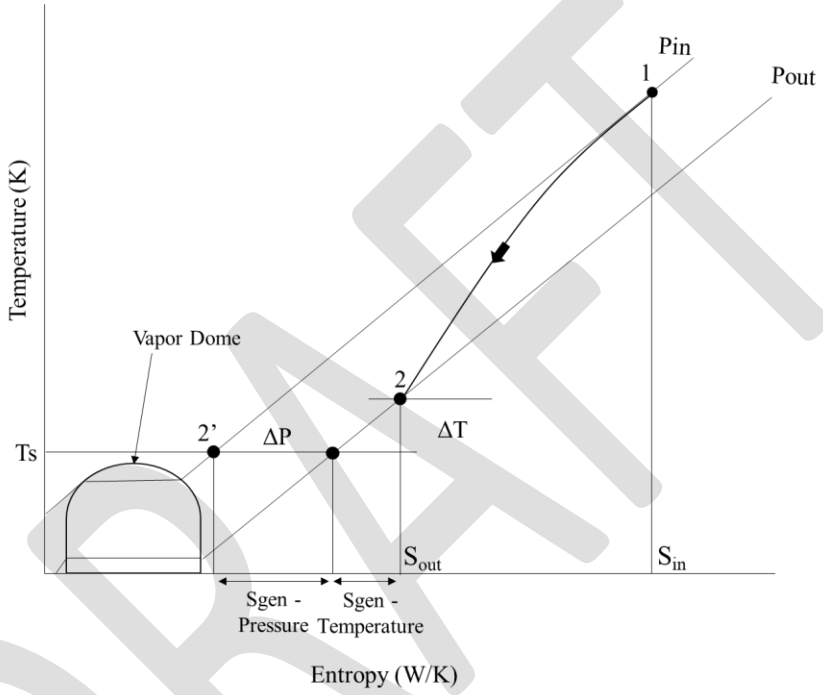

Figure 1: Entropy versus temperature diagram for cooling flow in a tube.

Combining the first and second laws of thermodynamics and applying the ideal gas assumption results in Equations 1 and 2 which are used to quantify the rate of entropy generation from the pressure and temperature differentials.

$$\dot{S}_{gen_{HT}} = \dot{m} C_p \frac{T_2 - T_{2'}}{T_{2'}} \tag{1}$$

$$\dot{S}_{gen_P} = \dot{m} R \frac{P_1 - P_2}{P_1} \tag{2}$$

Where $\dot{S}_{gen_{HT}}$ is the rate of entropy generation from heat transfer, $\dot{m}$ is the mass flow rate of the fluid, C_p is the heat capacity of the fluid at constant pressure, T is temperature, R is the ideal gas constant, and P is the pressure. Entropy generation from pressure increases with increasing tube length and that from heat transfer decreases. For a given system, summing the two modes of entropy generation yields a minimum point, representing an ideal aspect ratio. A system diagram of a tube containing a flowing fluid is shown in Figure 2. By discretizing the cooldown process into many small elements, the heat capacity can be assumed approximately constant across each element despite the change in temperature.

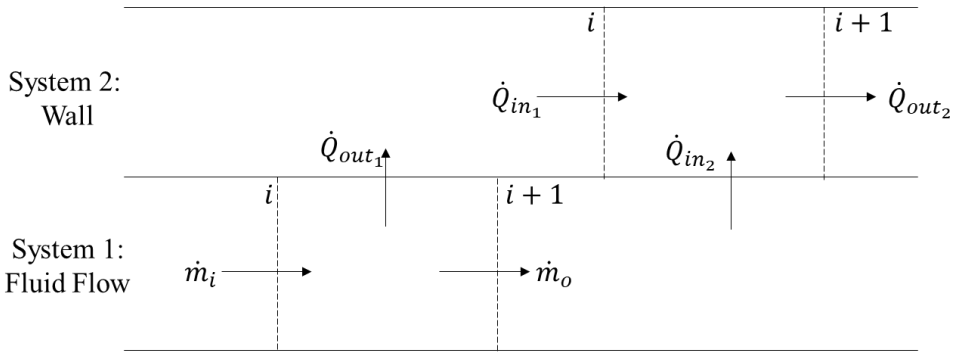

Figure 2: System diagram of flow through a tube.

An example of a point of minimum entropy generation is shown in Figure 3 for a tube with an inner diameter of 0.0127 m, a constant surface temperature of 200 K, a mass flow rate of 0.093 g/s, and a packed bed catalyst with a diameter of 300 micron. For simplicity, heat transfer along the length of the wall is not considered in this example.

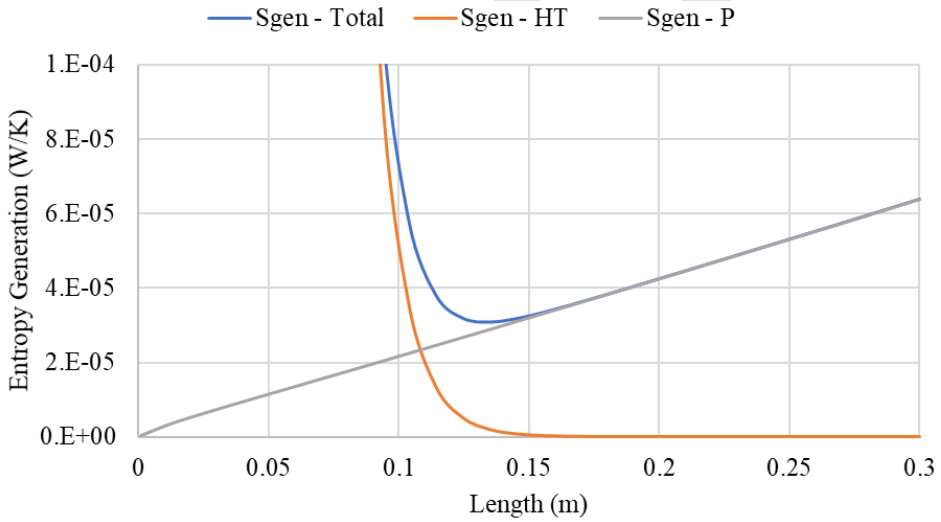

Figure 3: Length versus entropy generation from heat transfer and pressure drop, as well as the sum. A minimum point occurs near a length of 13 cm.

It is common for flows to require greater lengths than the optimal value so flows bifurcate to match cross-section aspect ratio with mass flow rate until a physical limitation is reached [13]. This results in an optimum design with minimum entropy generation as dictated by the Hess-Murray rule. This rule was developed for water-like biological circulatory systems, however, still holds for minimizing flow resistance in other systems. The parent-child ratio is allowed to vary from that of the Hess-Murray rule, $2^{1/3}$, to remain relevant for hydrogen liquefaction.

A model is created to simulate a branching tube network and the total entropy generation, the outlet pressure, and the outlet temperature are calculated assuming an inlet temperature of 293 K and an inlet pressure of 652.93 kPa. Ignoring heat transfer along the length of the wall and superimposing a linear temperature gradient along the surface, representing an ideal scenario, the outlet temperature, outlet pressure, and total entropy generation in the system decrease with increasing layers. The data is shown in

Table 1.

Table 1: Total entropy generation, output pressure, and final temperature of a branching tube system as a function of the number of layers.

Number of Layers	Total Entropy Generation (W/K)	Final Pressure (kPa)	Final Temperature (K)
1	13.500	648.095	156.00
2	9.614	647.640	118.70
3	6.533	648.091	87.82
4	6.403	646.962	65.57
5	6.064	646.970	51.04

The resulting geometry is shown in Table 2. Neither the lengths nor the diameters are consistent with the Hess-Murray Rule. The lengths of later layers are longer than those prior, and diameters remain fairly consistent between layers. This is due to the reduction in hydrogen viscosity as the flow is cooled. The minimum diameter and length are bounded at 0.003175 m and 0.001 m respectively.

Table 2: Lengths and diameters of a branching fluid system as a function of the number of layers.

Total Number of Layers		Layer 1	Layer 2	Layer 3	Layer 4	Layer 5
1	Length (m)	0.142				
	Diameter (m)	0.009525				
2	Length (m)	0.001	0.0141			
	Diameter (m)	0.003195	0.003175			
3	Length (m)	0.001	0.001	0.14		
	Diameter (m)	0.006747	0.009525	0.006038		
4	Length (m)	0.001	0.01013	0.01035	0.1205	
	Diameter (m)	0.0018	0.0022	0.003	0.0035	
5	Length (m)	0.001	0.01011	0.01046	0.01019	0.1102
	Diameter (m)	0.0018	0.0022	0.003	0.0035	0.003175

Next, heat transfer along the length of the wall is added to the model. The wall is used to determine the real temperature profile of the system and contains another mode of entropy generation. The wall thickness is varied according to an exponential function, shown in Equation 3.

$$th = x[i]^e + y \tag{3}$$

Where th is wall thickness, x[i] is the position along the length, e is the exponent, and y is the initial thickness. The resulting total rate of entropy generation and the outlet temperature of the fluid stream and wall are calculated. 110 W is removed from the bottom of the tube. The wall thickness is increased to account for decreasing thermal conductivity during cooling and siphoning of heat for removal. The total system entropy generation as a function of the wall thickness exponent is shown in Figure 4.

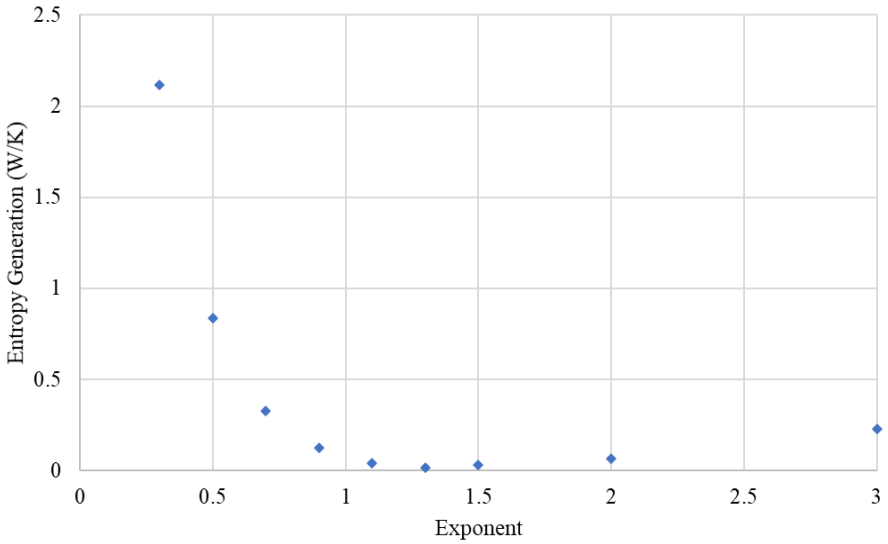

Figure 4: Total entropy generation of a tube containing a fluid as a function of the wall thickness equation exponent.

A point of minimum entropy generation occurs with an exponent of 1.3 as shown in Figure 4. This represents a scenario with optimum resistance to axial conduction and yields almost linear temperature profiles. In addition, the outlet temperature of both the fluid stream and wall decrease as the exponent is increased. In this scenario the assigned material is 6061 aluminum. The ideal exponent would vary if a different material were used.

The final heat exchanger design utilizes four layers for a final total of eight branches with an average wall thickness exponent of 2.125. The final entropy generation was determined using a Crank-Nicolson numerical integration technique with 50 elements per layer and implemented in Engineering Equation Solver [14].

The heat exchanger will be mounted to a dual stage Sumitomo RDK-415D cryogenic refrigerator. The heat exchanger fits onto the cryogenic refrigerator like a sleeve and must comply with the constraints listed in Table 3. In addition, the hydrogen is assumed to have equilibrium ortho-parahydrogen composition, and this assumption is validated by the application of a ruthenium oxide catalyst within the system. 6061 aluminium was selected for the design.

Table 3: System constraints, the bounded values, and the reason for each constraint.

Constraint	Bounded Value/s	Reason
Mass Flow Rate	18.8 SLPM	Maximum output of attached electrolyzer.
Wall Thickness	5.653 µm	Minimum value to prevent bursting.
	1 mm	Minimum value that can be printed.
Part Height	0.325 m	Maximum print height. This is a function of the printer used.
Height of Lower Heat Exchanger	0.239 m	Height between upper and lower stages of cryogenic refrigerator.
Height of Upper Heat Exchanger	0.0795 m	Difference between the maximum print height and the height of the lower heat exchanger.
Inner Diameter	3.175 mm – 9.525 mm	Below 3.175 mm printing powder cannot be removed from the system. Above 9.525 mm minimal heat transfer occurs.
Wall Thickness	1 cm	There is 12.7 mm of clearance between the upper stage of the cryogenic refrigerator and the dewar neck. Assuming an inner diameter of 3.175 mm, the maximum allowable wall thickness of the lower portion of the heat exchanger without interference is 1.00 cm.

The lower section of the heat exchanger must maximize the allowable inlet temperature while outputting hydrogen at the saturation temperature, simultaneously minimizing entropy generation. Maximizing the inlet temperature will maximize the heat load at the upper stage of the cryogenic refrigerator and therefore the mass flow rate. The lower section is assumed to contain no branching, and it is determined that eight branches can fit within system constraints. In all, the lower section of the heat exchanger contains eight tubes, all 0.239 m long with an inner diameter of 3.175 mm and a maximum wall thickness of 1 cm. The wall thickness equation exponent had to be increased above ideal to achieve the desired temperature gradients. This results in slightly convex temperature profiles.

The upper section of the heat exchanger must accept gaseous hydrogen at ambient temperature and output hydrogen near 100 K to be continuous with the lower stage. The lower stage contains eight tubes, and the system must begin with one, therefore the upper section contains four layers. This results in a design where all layers are 1 cm except for the last and the inner diameter remains consistent at 3.175 mm. Again, the wall thickness equation is increased above ideal. Table 4 shows the theoretical results.

Table 4: Theoretical system parameters for the upper and lower portions of the heat exchanger.

	Lower Portion	Upper Portion
Parameter	Value	
Hydrogen Inlet Temperature	100 K	293 K
Wall Inlet Temperature	95 K	292 K
Mass Flow Rate	0.008 g/s	0.008 g/s
Hydrogen Outlet Temperature	24.39 K	102 K
Wall Outlet Temperature	20.18 K	84.63 K
Wall Thickness Equation	$th[i]=0.3x[i]^{2.1}+0.0009$	$th[i]=x[i]^{2.15}+0.00043$
Inner Diameter	3.175 mm	3.175 mm
Total Length	0.239 m	0.0795 m
Rate of Entropy Generation	0.7087 W/K	0.6886 W/K

Traditionally, heat exchanger effectiveness is quantified using the LMTD or NTU-ε methods. These metrics compare the actual and ideal rates of heat transfer and rely on knowing the temperature profiles of the two fluids exchanging heat. In this scenario the temperature profile of the hydrogen is known but not that of the helium in the cryogenic refrigerator, therefore a new metric is defined. The new metric is shown in Equation 3, and the terms in Equation 3 are defined in Equations 4 and 5.

$$\mu = \frac{\dot{Q}_{ideal}}{\dot{Q}_{real}}, \qquad \dot{Q}_{ideal} = \dot{Q}_{H2} + \dot{Q}_{HEX} + \dot{Q}_{OP}, \qquad \dot{Q}_{real} = \dot{S}_{gen} T_f + \dot{Q}_{ideal} \tag{3-5}$$

Where μ is the effectiveness metric, $\dot{Q}_{ideal}$ is the ideal rate of heat transfer, $\dot{Q}_{real}$ is the real amount of heat transfer, $\dot{Q}_{H2}$ is the heat required to cool the hydrogen stream from ambient to liquefaction temperature, $\dot{Q}_{HEX}$ is the heat required to cool the heat exchanger to liquefaction temperature, $\dot{Q}_{OP}$is the heat of the ortho-para conversion, $\dot{S}_{gen}$ is the rate of entropy generation in the system, and T_f is the outlet temperature of the hydrogen. Using this metric, the effectiveness of the branching design is 0.6645.

The theoretical design is compared to a single tube design with a packed bed catalyst. After comparison between the branching and the single tube designs, the thermal mass of the branching design is estimated to be 43.8% less, the length is estimated to be 91.3% less, and the branching design is estimated to be 23.2% more effective. However, the additively manufactured design currently costs 206% more to manufacture than the single tube design.

3. Experiment

The branching heat exchanger is installed on the cryogenic refrigerator, mounted within the neck of a custom Cryofab liquid hydrogen dewar, and three Lakeshore XDT-670-CU-1.4L sensors are installed. There is one sensor on each flange of the heat exchanger and one in the outlet fluid flow. The mounted heat exchanger as well as the important components are shown in Figure 5.

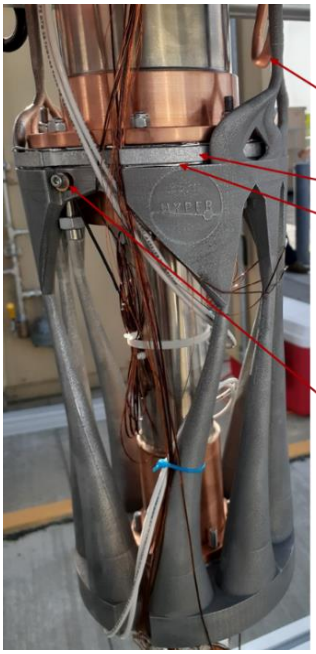

System Components:

- 122 copper tubing
- 6061 aluminum spacer plate
- Indium foil
- 316 stainless steel socket headed cap screws
  - M5 for the cryocooler and M3 for the temperature sensors
- Belleville washers
- Brass Swagelok fittings
- Lakeshore XDT-670-CU-1.4L temperature sensors
- Ruthenium(iii) chloride

Figure 5: Heat exchanger mounted to the cryogenic refrigerator with key features listed.

Although the system is designed for 6061 aluminium, no manufacturers were comfortable completing the print given the current available technology. Instead, the part was printed in $AlSi_{10}Mg$ which has unknown thermal properties below 230 K. Based on the known values, a decrease in system performance of about 30% is estimated using linear extrapolation. Also, permanent support material was added to support some of the features during printing. The support material has an unknown impact on the system performance.

The first metric used to quantify system performance is the mass flow rate. To determine this value a buffer tank is installed prior to the heat exchanger and the change is pressure is monitored over time. The average rate of liquefaction is determined to be 0.0035 g/s, which is 44.2% of the value predicted using theoretical modelling. The uncertainty associated with the pressure readings is ±3.447 kPa. The calculated rates of liquefaction are shown in Table 5.

Table 5: Measured rates of liquefaction.

	Rate of Liquefaction (g/s)
Charge 1	0.0038
	0.0038
	0.0037
Charge 2	0.0034
	0.0035
	0.0034
Charge 3	0.0031

The second metric used to quantify system performance is the temperature profile. The upper flange is shown to maintain a temperature of 58.05 K, the lower flange a temperature of 26.16 K, and the inlet temperature is assumed to be ambient. The uncertainty associated with the temperature readings is ±12 mK. The lower stage reaches liquefaction temperatures as predicted and the upper stage resides about 45 K lower than predicted.

The following are a list of reasons why the mass flow and temperature of the upper stage are lower than expected.

- The thermal properties of the heat exchanger are unknown and likely lower than the system was designed for, resulting in increased resistance to axial conduction. If the thermal properties were low, the achievable temperature gradient in the lower portion of the heat exchanger would

decrease, lowering the temperature of the upper stage and the overall heat load of the system. Thereby decreasing the mass flow rate.

- A spacer plate was added between the upper flange of the heat exchanger and the upper stage of the cryogenic refrigerator to achieve contact. This likely resulted in decreased thermal contact and increased resistance, decreasing heat transfer and therefore the allowable mass flow rate.
- There may not be adequate pressure applied to the indium foil, which would drastically increase the resistance to heat transfer. The expected pressure is 10 kg of force.

4. Conclusions and Future Work

A minimum entropy heat exchanger is designed and built with a branching structure and varying wall thickness. The heat exchanger is mounted to a dual stage Gifford-McMahon cryogenic refrigerator and used to liquefy hydrogen. The system is additively manufactured with $AlSi_{10}Mg$ but designed to be printed in 6061 aluminium. Theoretical calculations estimate a 23.2% improvement in system effectiveness when compared to a single tube design. The optimized design also decreases the length and thermal mass of the system by 91.3% and 43.8% respectively when compared to the single tube design. Results indicate a mass flow rate 44.19% of the predicted value and the temperature of the upper stage of the cryogenic refrigerator is about 45 K lower than anticipated. Liquefaction is achieved. For future work it is recommended that the heat exchanger be printed out of a more optimum material, which is defined as one with a high thermal conductivity, low heat capacity, and low density. In addition, it is recommended that the thermal contraction that occurs as a result of printing is quantified to eliminate the need for a spacer plate. Support material should also be minimized.

5. References

[1] Quack H 2002 Conceptual design of a high efficiency large capacity hydrogen liquefier. In: *AIP Conference Proceedings*: American Institute of Physics pp 255-63

[2] Cardella U, Decker L, Sundberg J and Klein H 2017 Process optimization for large-scale hydrogen liquefaction *International Journal of Hydrogen Energy* **42** 12339-54

[3] Baker C and Shaner R 1978 A study of the efficiency of hydrogen liquefaction *International Journal of Hydrogen Energy* **3** 321-34

[4] Farzaneh-Gord M, Ameri H and Arabkoohsar A 2016 Tube-in-tube helical heat exchangers performance optimization by entropy generation minimization approach *Applied Thermal Engineering* **108** 1279-87

[5] Popov D, Fikiin K, Stankov B, Alvarez G, Youbi-Idrissi M, Damas A, Evans J and Brown T 2019 Cryogenic heat exchangers for process cooling and renewable energy storage: A review *Applied Thermal Engineering* **153** 275-90

[6] Timmerhaus K and Schoenhals R 1995 *Advances in Cryogenic Engineering*: Springer pp 445-62

[7] Ahmadi P, Hajabdollahi H and Dincer I 2011 Cost and entropy generation minimization of a cross-flow plate fin heat exchanger using multi-objective genetic algorithm *Journal of heat transfer* **133**

[8] Babaelahi M, Sadri S and Sayyaadi H 2014 Multi-Objective Optimization of a Cross-Flow Plate Heat Exchanger Using Entropy Generation Minimization *Chemical Engineering & Technology* **37** 87-94

[9] Sahiti N, Krasniqi F, Fejzullahu X, Bunjaku J and Muriqi A 2008 Entropy generation minimization of a double-pipe pin fin heat exchanger *Applied Thermal Engineering* **28** 2337-44

[10] Zhou Y, Zhu L, Yu J and Li Y 2014 Optimization of plate-fin heat exchangers by minimizing specific entropy generation rate *International Journal of Heat and Mass Transfer* **78** 942-6

[11] Raymond J 2021 Entropy Optimization of an Additively Manufactured Heat Exchanger with a Dual Stage Gifford-McMahon Cryogenic Refrigerator for Hydrogen Liquefaction. In: *School of Mechanical and Materials Engineering*: Washington State University p 171

[12] Radebaugh R 2015 The Role of Cryogenics in the U.S. Hydrogen Bomb Program and Vise Versa. National Institute of Standards and Technology

[13] Bejan A 2016 *Advanced engineering thermodynamics*: John Wiley & Sons

[14] 2021 Engineering Equation Solver.

[15] Raymond J and Leachman J 2021 Novel Heat Exchanger for Staged Cryogenic Refrigerators. (United States of America)

Acknowledgments
The authors would like to thank the engineers at Elementum 3D for providing guidance on how to make a printable design. The authors would also like to thank the Department of Defense and the Donna Jung Scholarship Award for providing funding for this research, as well as the Voiland College of Engineering and Architecture at Washington State University for support of this work [15].